Received 28 July 2024; accepted 14 August 2024. Date of publication 22 August 2024; date of current version 4 September 2024.

Digital Object Identifier 10.1109/OJCOMS.2024.3447839

Joint Power Control and Pilot Assignment in Cell-Free Massive MIMO Using Deep Learning

MUHAMMAD USMAN KHAN (Member, IEEE), ENRICO TESTI (Member, IEEE), MARCO CHIANI (Fellow, IEEE), AND ENRICO PAOLINI (Senior Member, IEEE)

CNIT/WiLab, DEI, University of Bologna, 47521 Cesena, Italy

CORRESPONDING AUTHOR: E. TESTI (e-mail: enrico.testi@unibo.it)

This work was supported in part by the Consorzio Nazionale Inter-Universitario per le Telecomunicazioni (CNIT) Wireless Communications Laboratory (WiLab) and the WiLab-Huawei Joint Innovation Center; and in part by the European Union through the Italian National Recovery and Resilience Plan of NextGenerationEU, Partnership on "Telecommunications of the Future" under Grant PE00000001-RESTART.

ABSTRACT Cell-free massive MIMO (CF-mMIMO) networks leverage seamless cooperation among numerous access points to serve a large number of users over the same time/frequency resources. This paper addresses the challenges of pilot and data power control, as well as pilot assignment, in the uplink of a cell-free massive MIMO (CF-mMIMO) network, where the number of users significantly exceeds that of the available orthogonal pilots. We first derive the closed-form expression of the achievable uplink rate of a user. Subsequently, harnessing the universal function approximation capability of artificial neural networks, we introduce a novel multi-task deep learning-based approach for joint power control and pilot assignment, aiming to maximize the minimum user rate. Our proposed method entails the design and unsupervised training of a deep neural network (DNN), employing a custom loss function specifically tailored to perform joint power control and pilot assignment, while simultaneously limiting the total network power usage. Extensive simulations demonstrate that our method outperforms the existing power control and pilot assignment strategies in terms of achievable network throughput, minimum user rate, and per-user energy consumption. The model versatility and adaptability are assessed by simulating two different scenarios, namely a urban macro (UMa) and an industrial one.

INDEX TERMS Cell-free massive MIMO, deep learning, pilot assignment, power control.

I. INTRODUCTION

AS THE demands for device connectivity and mobile data traffic escalate, strategic base station (BS) densification within the network emerges as a pivotal solution [1]. Network densification can be achieved in two ways: adding more BSs for local spectrum reuse or implementing massive multiple-input multiple-output (mMIMO) to reduce interference [2], [3]. The first architecture that combines the advantages of both approaches was proposed in [4], known as cell-free massive MIMO (CF-mMIMO). The CF-mMIMO can achieve the objectives of 6G by improving the (usually poor) quality of service for the users at the edge of the cell and reducing inter-cell interference [5]. In such a distributed mMIMO-based network, a large number of service antennas, called access points (APs), serve a group of users distributed in a wide area. Unlike conventional cellular networks, this approach discards the concept of cells and cell boundaries entirely. The CF-mMIMO approach relies on seamless cooperation among numerous APs, all operating within the same time-frequency resource using time-division duplexing (TDD). At the center of the network is the central processing unit (CPU) through which the cooperation between the APs takes place. The APs are connected to the CPU through a fronthaul connection. Such network architecture, augmented by emerging technologies like reflective intelligent surfaces (RISs), extremely large-scale MIMO (XL-MIMO), and holographic MIMO, is among the most promising candidates for next-generation wireless networks [6], [7], [8], [9].

With reference to massive machine-type communications (mMTC) services, a typical massive multiple access (MMA) problem arises in the uplink, in which a myriad

of devices physically located in the same area contend to transmit their packets, consisting of a pilot and data payload, over the radio access network. Due to limited coherence time intervals and a very large number of devices, assigning orthogonal pilots to every user becomes impractical [3]. Consequently, we are compelled to reuse pilots, inadvertently giving rise to the pilot contamination phenomenon, which deteriorates the quality of channel estimation [10]. Additionally, the challenge of inter-user interference emerges, demanding innovative solutions, e.g., using advanced power control mechanisms. However, the mMIMO system benefits from channel hardening, i.e., the effect of small-scale fading becomes negligible at the receiver due to the presence of multiple antennas. This allows us to optimize power coefficients based on the large-scale fading coefficients instead of small-scale fading which requires frequent updates [11].

Strategic power control and careful pilot assignment are pivotal in mitigating inter-user interference and enhancing network performance. The most diffused power control strategies focus on maximizing the minimum user rate to ensure uniform service quality regardless of the spatial user distribution [4], [12], [13]. The max-min problem for power/pilot assignment can be solved through optimization [14], [15], [16]. However, the high computational burden inherent in optimization algorithms poses substantial challenges in terms of meeting stringent time constraints, making classical optimization techniques impractical. Leveraging the universal function approximation capability of artificial neural networks (ANNs), deep learning (DL)-based methodologies emerge as an innovative solution yielding high performance while simultaneously reducing computational complexity, when compared to traditional optimization algorithms [17]. Indeed, whereas an optimization algorithm necessitates to be re-run from scratch whenever a system parameter or input variable changes, once the DL model is trained, we can exploit its forward propagation for fast and efficient prediction.

A. RELATED WORKS

1) POWER CONTROL

The advantages offered by DL algorithms have catalyzed a significant body of work in CF-mMIMO [18], [19], [20], [21]. Power control in the CF-mMIMO scenario is no exception [5], [17], [22], [23], [24]. The approaches for power control through DL in the literature can be divided into two: supervised and unsupervised. In supervised learning, a crucial requirement is the availability of output labels (specifically, the power coefficients of each user) for both training and testing the network. The output labels are generated using optimization algorithms, requiring significant execution time. A supervised long short-term memory (LSTM) network and a deep neural network (DNN) for power control is proposed in [5] and [22], respectively, feeding the position of the users as input to the learning model. In [17], a DNN that takes the large-scale fading coefficients as input and produces the optimized power coefficients and the total power budget as output is proposed.

Conversely, in unsupervised learning, no prior knowledge of output labels is required. This reduces the time to generate the datasets but necessitates the development of a problem-tailored loss function. In [23], [24], a specific loss function that maximizes the minimum user rate is proposed. In [25], the model complexity is reduced by feeding aggregated large-scale fading coefficients to the DNN, rather than individual ones. Notably, the DNN with the proposed loss function achieves better performance than the optimization algorithm in [4]. In [26], a soft max-min problem is proposed. Most of the above-mentioned strategies presume that mutually orthogonal pilots are assigned to the users. Yet, in massive access scenarios, this approach becomes impractical due to the limited coherence intervals.

2) PILOT ASSIGNMENT

A substantial body of research has explored pilot assignment strategies, with random pilot assignment emerging as the most widely recognized approach [27]. A repulsive clustering-based method for the pilot assignment in CF-mMIMO is proposed in [28]. Graph coloring-based pilot assignment is presented in [29]. The study in [10] is focused on forming groups of the users and APs to reduce pilot contamination. A supervised learning-based approach that maps the users' location to a pilot sequence is presented in [30]. A multi-agent reinforcement learning-based approach for pilot assignment is proposed in [3].

3) POWER CONTROL AND PILOT ASSIGNMENT

Only few works in the literature address both power control and pilot assignment simultaneously. In [4], a greedy iterative algorithm is proposed that assigns a different pilot to the user having the minimum user rate while solving the power control problem via bisection. Mai et al. designed pilots and formulated optimization problems for joint pilot power and data power control [31]. In [16], a pilot assignment strategy is proposed focusing on active users detection (AUD), and then they developed a power control scheme for coexisted human-type communication (HTC) and machine-type communication (MTC) traffic. In [32], a deep reinforcement learning (DRL)-based approach for joint power and pilot assignment is presented. The authors perform clustering of the users and then assign pilots and allocate power using DRL, to increase AUD performance.

B. MAIN CONTRIBUTIONS

The literature predominantly emphasizes either power control or pilot assignment tasks, with limited attention given to both optimizations. Even in cases where both optimizations are addressed, most studies rely on time-inefficient optimization algorithms. Although there are works exploring DRL for joint power control and pilot assignment, they tend to concentrate on AUD rather than enhancing the spectral efficiency (SE), leaving room for more comprehensive and

efficient methodologies in this domain. Thus, the main contributions of the paper are summarised as follows.

- We propose a multi-task learning framework consisting of a DNN for joint pilot and data power control and pilot assignment (JPDCPA). The network is trained in an unsupervised manner by means of a custom loss function, designed to maximize the minimum user rate in a CF-mMIMO network.
- We consider a massive access scenario consisting of a large number of users to which a much smaller number of orthogonal pilots must be assigned. The multi-task DNN is designed to be scalable and to deal with large cell-free networks.
- We validate the proposed model via extensive simulation, providing a comparison with state-of-the-art methods in terms of achievable network throughput, minimum user rate, and energy consumption of the devices after optimization.
- We demonstrate the versatility and adaptability of our approach by assessing its performance in urban macro (UMa) and indoor industrial scenarios [33]. Furthermore, in our study we have considered different user-to-antenna ratios, including scenarios where the number of users exceeds that of the antennas, and vice versa.
- We characterize the performance of the proposed DNN in terms of the minimum user rate and per-user uplink throughput rate. Additionally, we evaluate the network energy consumption and provide insights into the impact of each term in the custom loss function on the overall system performance.
- Finally, we investigate the computational complexity of the proposed approach in terms of floating point operations (FLOPs).

The rest of the paper is organized as follows. In Section II, we present the system model and in Section III, we present the signal-to-interference-plus-noise ratio (SINR) analysis. We formulate the problem for maximizing the minimum SINR in Section IV. The DL-based approach for joint pilot and data power control and pilot assignment in CF-mMIMO is described in Section V. Simulation setup along with the numerical results is provided in Section VI. Conclusions are drawn in Section VII.

Matrices, vectors, and scalars are represented by boldface uppercase, boldface lowercase, and lowercase letters, respectively. The fields of real and complex numbers are denoted by $\mathbb{R}$ and $\mathbb{C}$, respectively. The operations $(\cdot)^T$, $(\cdot)^*$, and $(\cdot)^H$ denote the transpose, conjugate, and conjugate transpose, respectively. The expectation and Euclidean norm operators are defined as $\mathbb{E}[\,\cdot\,]$ and $\|\cdot\|^2$, respectively. The normal and circularly-symmetric complex normal distributions with mean 0 and variance σ^2 are denoted by $\mathcal{N}(0,\sigma^2)$ and $\mathcal{CN}(0,\sigma^2)$, respectively.

This paper is an extension of [34]. While [34] focused exclusively on data power control and pilot assignment in a scenario with single-antenna APs, the current work expands on this foundation by considering pilot power control and multiple antennas APs. To incorporate pilot power control and multiple antennas, a new expression is derived for the achievable uplink rate of a user in a CF-mMIMO scenario and a new DNN architecture is proposed with a customized loss function. Unlike [34], which exclusively provides simulation results for the UMa scenario, this work considers also an industrial indoor one [33]. In [34], we focused on scenarios where the number of users exceeds the number of antennas. In this work, we extend the discussion to encompass scenarios where the number of users is fewer than the number of antennas. We introduce results that elucidate the significance of each loss term within the loss function. Furthermore, a comprehensive analysis of the algorithm's computational complexity is provided.

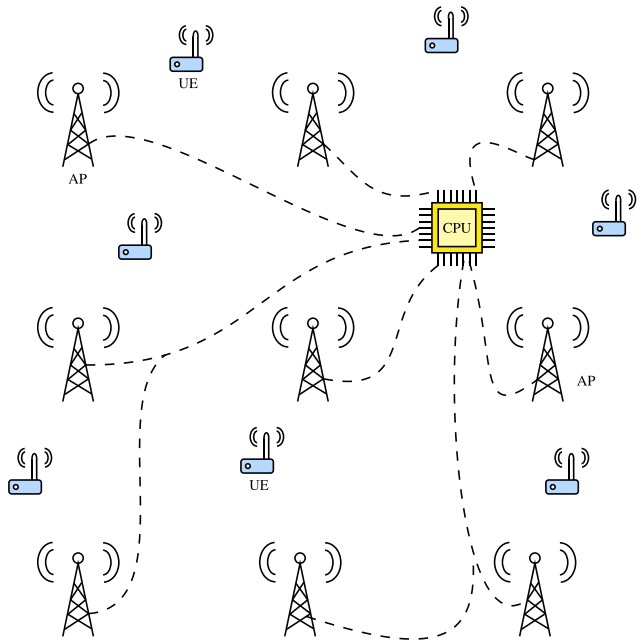

FIGURE 1. An illustration of a typical cell-free massive MIMO network.

II. SYSTEM MODEL

We consider a CF-mMIMO system with M APs, each equipped with N antennas, arranged on a grid and K users randomly deployed in an area measuring $D \times D$ m^2, as illustrated in Fig. 1. The APs are connected to a CPU through fronthaul links. We assume that the number of mutually orthogonal pilot sequences P is far less than the number of users K, i.e., $P \ll K$. The set of available orthogonal pilot sequences is denoted by $\mathcal{P} = \{\boldsymbol{p}_1, \boldsymbol{p}_2, \ldots, \boldsymbol{p}_P\}$. We assume that the large-scale fading coefficients between every user and AP are known at the CPU whenever necessary [17], [23], [25]. We assume that the APs serve all the users in the same time-frequency resources and that each channel coherence interval is divided into downlink and uplink phases, such that the system operates in TDD.

We also assume that during the downlink phase the CPU communicates the optimized power coefficients and pilot assignments to the users of the network through the APs.

A. UPLINK TRANSMISSION

The uplink transmission consists of two phases: pilot transmission and data transmission.

1) PILOT TRANSMISSION

In this phase, all K users synchronously transmit the pilot they have been assigned to via optimization. The vector of received symbols at nth antenna of the mth AP, $\boldsymbol{y}_{mn} \in \mathbb{C}^{\tau \times 1}$, is

$$\boldsymbol{y}_{mn} = \sqrt{\tau \rho_{\mathrm{p}}} \sum_{k=1}^{K} \sqrt{b_k} g_{mnk} \boldsymbol{\phi}_k + \boldsymbol{w}_{mn} \tag{1}$$

where ρ_{p} is the normalized pilot signal-to-noise ratio (SNR), $\boldsymbol{\phi}_k \in \mathbb{C}^{\tau \times 1}$ are the pilot symbols transmitted by user k with $\|\boldsymbol{\phi}_k\|^2 = 1$, τ is the pilot sequence length, $b_k \in [0, 1]$ is the pilot power control coefficient, g_{mnk} is the channel coefficient between the kth user and the nth antenna of the mth AP, and $\boldsymbol{w}_{mn} \in \mathbb{C}^{\tau \times 1}$ is additive noise and its elements are independent and identically distributed (i.i.d.) $\mathcal{CN}(0, 1)$ random variables (r.v.s). The normalized pilot transmit SNR is defined as

$$\rho_{\mathrm{p}} = \frac{\bar{\rho}_{\mathrm{p}}}{\sigma_n^2} \tag{2}$$

where $\sigma_n^2 = Bk_B T_0 \mathrm{NF}$, $\bar{\rho}_{\mathrm{p}}$ is the pilot transmit power, B is the bandwidth, k_B is the Boltzmann constant, T_0 is the equivalent noise temperature, and NF denotes the noise figure of the receiver. The channel coefficient between user k and at the nth antenna at the mth AP is modeled as

$$g_{mnk} = \sqrt{\beta_{mk}} h_{mnk} \tag{3}$$

where β_{mk} is the large-scale fading incorporating both path-loss and log-normal shadowing, and $h_{mnk} \sim \mathcal{CN}(0, 1)$ is the small-scale fading. The large-scale fading coefficient is

$$\beta_{mk} = \frac{10^{\sigma_{\mathrm{sh}} s_{mk}/10}}{\mathrm{PL}_{mk}} \tag{4}$$

where PL_{mk} is the path-loss from the kth user to the mth AP, σ_{sh} is the shadowing intensity, and $s_{mk} \sim \mathcal{N}(0, 1)$. The nth antenna at the mth AP estimates the channel associated with the kth user by projecting $\boldsymbol{y}_{mn}$ along $\boldsymbol{\phi}_k$, as

$$\begin{aligned} \tilde{y}_{mnk} &= \boldsymbol{\phi}_k^H \boldsymbol{y}_{mn} \\ &= \sqrt{\tau \rho_{\mathrm{p}}} \left(\sqrt{b_k} g_{mnk} + \sum_{k' \neq k}^{K} \sqrt{b_{k'}} g_{mnk'} \boldsymbol{\phi}_k^H \boldsymbol{\phi}_{k'} \right) + \boldsymbol{\phi}_k^H \boldsymbol{w}_{mn} \end{aligned} \tag{5}$$

such that the minimum mean square error (MMSE) channel estimate is

$$\begin{aligned} \hat{g}_{mnk} &= \frac{\mathbb{E}\left[\tilde{y}_{mnk}^* g_{mnk}\right]}{\mathbb{E}\left[|\tilde{y}_{mnk}|^2\right]} \tilde{y}_{mnk} \\ &= c_{mk} \tilde{y}_{mnk} \end{aligned} \tag{6}$$

where c_{mk} is defined as

$$c_{mk} = \frac{\sqrt{\tau \rho_{\mathrm{p}} b_k} \beta_{mk}}{\tau \rho_{\mathrm{p}} \sum_{k'=1}^{K} b_{k'} \beta_{mk'} |\boldsymbol{\phi}_k^H \boldsymbol{\phi}_{k'}|^2 + 1}. \tag{7}$$

Let us remark that the quality of the channel estimate depends on the pilots assigned to all the users of the network.

2) UPLINK DATA TRANSMISSION

The uplink phase is then concluded with the simultaneous transmission of the data payload of all the users. The generic received signal sample at the nth antenna of the mth AP can be written as

$$z_{mn} = \sqrt{\rho} \sum_{k=1}^{K} \sqrt{q_k} g_{mnk} x_k + \nu_{mn} \tag{8}$$

where ρ is the normalized data transmit SNR, $q_k \in [0, 1]$ is the power control coefficient of user k, x_k is the data payload symbol transmitted by user k with $\mathbb{E}[|x_k|^2] = 1$, and $\nu_{mn} \sim \mathcal{CN}(0, 1)$ is additive noise. The normalized data transmit SNR is defined as

$$\rho = \frac{\bar{\rho}}{\sigma_{\mathrm{n}}^2} \tag{9}$$

where $\bar{\rho}$ is the maximum data transmit power.

We assume that for the detection of the symbols transmitted by the kth user each AP processes the received signal by multiplying it with the complex conjugate of the locally derived channel estimate [4]. The resultant quantity is then forwarded to the CPU through a fronthaul link to perform joint detection. The aggregated received signal at the CPU is

$$\begin{aligned} r_k &= \sum_{m=1}^{M} \sum_{n=1}^{N} \hat{g}_{mnk}^* z_{mn} \\ &= \sqrt{\rho} \sum_{k'=1}^{K} \sum_{m=1}^{M} \sum_{n=1}^{N} \sqrt{q_{k'}}\, \hat{g}_{mnk}^* g_{mnk'} x_{k'} + \sum_{m=1}^{M} \sum_{n=1}^{N} \hat{g}_{mnk}^* \nu_{mn}. \end{aligned} \tag{10}$$

III. SINR ANALYSIS

In this section, we obtain a closed-form expression for the uplink achievable rate using the formulation introduced in [4], [15]. A key distinction between our proposed method and the approach outlined in [4], [15] pertains to pilot power allocation. The two approaches assume equal pilot power allocation for each user, while we perform also pilot power control. The derivation of the achievable rate expression assumes that each user possesses knowledge of channel statistics but not specific channel realizations. The received signal r_k can be expressed as

$$r_k = \mathrm{DS}_k x_k + \mathrm{BU}_k x_k + \sum_{k' \neq k}^{K} \mathrm{IUI}_{kk'} x_k + \mathrm{TN}_k \tag{11}$$

where

$$\mathrm{DS}_k \triangleq \sqrt{\rho}\,\mathbb{E}\left\{\sum_{m=1}^{M}\sum_{n=1}^{N}\sqrt{q_k}g_{mnk}\hat{g}^*_{mnk}\right\}, \tag{12}$$

$$\mathrm{BU}_k \triangleq \sqrt{\rho}\sum_{m=1}^{M}\sum_{n=1}^{N}\sqrt{q_k}g_{mnk}\hat{g}^*_{mnk} - \sqrt{\rho}\,\mathbb{E}\left\{\sum_{m=1}^{M}\sum_{n=1}^{N}\sqrt{q_k}g_{mnk}\hat{g}^*_{mnk}\right\} \tag{13}$$

$$\mathrm{IUI}_{kk'} \triangleq \sqrt{\rho}\sum_{m=1}^{M}\sum_{n=1}^{N}\sqrt{q_{k'}}g_{mnk'}\hat{g}^*_{mnk} \tag{14}$$

$$\mathrm{TN}_k \triangleq \sum_{m=1}^{M}\sum_{n=1}^{N}\hat{g}^*_{mnk}\nu_{mn}. \tag{15}$$

The terms DS_k, BU_k, $\mathrm{IUI}_{kk'}$, and TN_k denote the desired signal for the kth user, the uncertainty in beamforming gain for the kth user, the inter-user interference introduced by the k'th user, and the total noise, respectively. The first term of (11) demonstrates no correlation with the second, third, and fourth terms, i.e., the desired signal and effective noise terms are uncorrelated. By considering uncorrelated Gaussian noise as a worst-case scenario, the achievable SINR of the received signal of the kth user can be expressed as

$$\mathrm{SINR}_k = \frac{|\mathrm{DS}|_k^2}{\mathbb{E}\{|\mathrm{BU}_k|^2\} + \sum_{k'\neq k}^{K}\mathbb{E}\{|\mathrm{IUI}_{kk'}|^2\} + \mathbb{E}\{|\mathrm{TN}_k|^2\}}. \tag{16}$$

By manipulating the expressions in (12), (13), (14), (15) and substituting them into (16), we derive the final expression for the achievable uplink rate of the kth user in (19), shown at the bottom of the page. Please refer to the Appendix for the complete proof.

IV. PROBLEM FORMULATION

In [4], the authors have demonstrated that uniform and good-quality service can be ensured to all the users of a CF-mMIMO system via max-min power control. Let us define the kth user uplink throughput rate as

$$R_k = \log_2(1 + \mathrm{SINR}_k) \tag{17}$$

where the SINR of user k is given by (19) and $\gamma_{mk} = \sqrt{\tau\rho_{\mathrm{p}}b_k}\beta_{mk}c_{mk}$ [4]. The max-min power control aims at maximizing the minimum user uplink throughput rate such that all the users of the network can experience good quality of service. In this work, we assume that the number of orthogonal pilots is considerably smaller than the total number of users, such that orthogonal pilots reuse becomes necessary. Adding such a constraint, the max-min problem can be formulated as

$$\begin{aligned}\max_{b_k,q_k,\boldsymbol{\phi}_k}\ & \min_k R_k \\ \text{s.t.}\ & 0 \le b_k \le 1, \quad k = 1,2,\ldots,K, \\ & 0 \le q_k \le 1, \quad k = 1,2,\ldots,K, \\ & \boldsymbol{\phi}_k \in \mathcal{P}.\end{aligned} \tag{18}$$

V. DEEP LEARNING-BASED APPROACH

In this section, we introduce a multi-task DNN designed to solve the problem in (18), allocating pilot and data power coefficients b_k and q_k, respectively, and simultaneously assigning pilot sequences $\boldsymbol{\phi}_k$ to the users. The proposed algorithm maximizes the minimum user rate based on the large-scale fading experienced by the users, which are known at the CPU [17], [23], [25]. Hereafter, we describe the data pre-processing strategy, the architecture of the proposed DL model, and the loss function used for the unsupervised training.

A. PRE-PROCESSING

To make unsupervised training effective and decrease the input layer size, we pre-processed the data by aggregating the large-scale fading coefficients and applying proper normalization. The data pre-processing procedure is detailed in the following.

1) **Large-scale fading coefficients aggregation:** We aggregate the large-scale fading coefficients related to user k as

$$\beta_k^{(j)} = \sum_{i=1}^{M}\beta_{ik}^{(j)} \tag{20}$$

where the superscript (j) refers to the jth sample of the dataset. This operation reduces the input layer size of the DL model, making the architecture scalable and suitable for large networks [25].

2) **Logarithmic scale conversion and scaling:** We perform z-score normalization of the aggregated fading coefficients in logarithmic scale, $\xi_k^{(j)} = \log_{10}(\beta_k^{(j)})$, such that the normalized data are zero mean and have standard deviation one, i.e.,

$$\eta_k^{(j)} = \frac{\xi_k^{(j)} - \bar{\mu}}{\bar{\sigma}} \tag{21}$$

where $\bar{\mu}$ and $\bar{\sigma}$ are the sample mean and sample standard deviation of $\xi_k^{(j)}$, respectively, computed over all the network users and the training samples. Let us remark that the test dataset is normalized using $\bar{\mu}$ and $\bar{\sigma}$ calculated over the training dataset.

$$\mathrm{SINR}_k = \frac{q_k N\left(\sum_{m=1}^{M}\gamma_{mk}\right)^2}{\sum_{k'\neq k}^{K}q_{k'}\left(\sum_{m=1}^{M}\gamma_{mk}\frac{\sqrt{b_{k'}}\beta_{mk'}}{\sqrt{b_k}\beta_{mk}}\right)^2|\boldsymbol{\phi}_k^H\boldsymbol{\phi}_{k'}|^2 + \sum_{k'=1}^{K}q_{k'}\sum_{m=1}^{M}\gamma_{mk}\beta_{mk'} + \frac{1}{\rho}\sum_{m=1}^{M}\gamma_{mk}}. \tag{19}$$

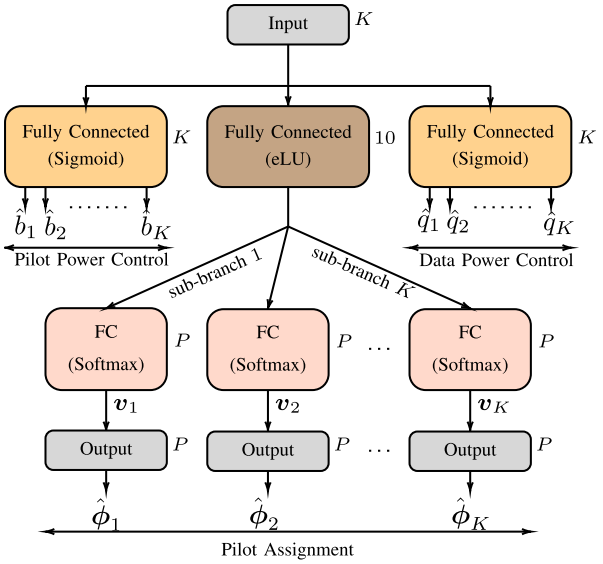

FIGURE 2. Model layout of the multi-task DNN for joint pilot and data power control and pilot assignment (JPDCPA). The size of each layer is specified next to it; for instance, the fully connected layers of the pilot and data power control branches contain *K* neurons each, while the output layer of a single pilot assignment sub-branch contains *P* neurons.

3) **Normalization:** We apply L^2-normalization to each sample of the dataset, such that the kth normalized feature of the jth sample is

$$\chi_k^{(j)} = \frac{\eta_k^{(j)}}{\sqrt{\sum_{i=1}^{K}\left(\eta_i^{(j)}\right)^2}}. \tag{22}$$

B. ARCHITECTURE

In this subsection, we present the proposed multi-task DNN architecture for joint pilot and data power control, and pilot assignment, which we refer to as JPDCPA. We explored various architectures by varying the numbers, types, and sizes of layers, aiming to identify an architecture that strikes a good balance between complexity and performance. Our experiments revealed that an excessive increase in the number of hidden layers of the multi-task DNN induces the phenomenon of gradient vanishing, and this is due to the unsupervised nature of the training process [35]. Thus, we chose an architecture capable of delivering remarkably high performance while maintaining a limited number of hidden layers. The input of the multi-task DNN is the vector of aggregated and pre-processed large-scale fading coefficients obtained from (22), while the outputs are the pilot and data power control coefficients, and the pilot indexes for each network user. The architecture comprises three branches, each of which performs one task as shown in Fig. 2. The power control branches perform regression tasks, while the pilot assignment one performs a classification task and is organized into K sub-branches, each responsible for the allocation of a pilot to a specific user. The DL model consists of fully connected layers with multiple neurons, each receiving multiple inputs as follows

$$\boldsymbol{z} = \boldsymbol{W}\boldsymbol{\alpha} + \boldsymbol{\varrho} \tag{23}$$

$$\boldsymbol{\alpha} = f(\boldsymbol{z}) \tag{24}$$

where $\boldsymbol{W} \in \mathbb{R}^{\text{out}\times\text{in}}$ is the weight matrix. Here, out and in represent the number of output and input features, respectively. The input to the layer is represented by $\boldsymbol{\alpha} \in \mathbb{R}^{\text{in}\times 1}$, and the bias is denoted by $\boldsymbol{\varrho} \in \mathbb{R}^{\text{out}\times 1}$ [35]. The non-linear activation function is denoted by $f(\cdot)$. This function enables the network to learn non-linear relations between input and output, a crucial aspect of DL models. The number of neurons employed in each fully connected layer is specified in Fig. 2. For instance, the number of neurons in the fully connected layer of the pilot power control branch is equal to K. Different non-linear activation functions have been used for the network layers depending on their purpose. The activation functions are applied element-wise to the layer input vectors, whose ith element is generically denoted by a_i. The sigmoid function is used in the pilot and data power control branches such that the optimized pilot (or data) power coefficient, $\hat{b}_i$ (or $\hat{q}_i$), for user i is

$$\hat{b}_i = \sigma(a_i) = \frac{1}{1+e^{-a_i}}. \tag{25}$$

We employ the exponential linear unit (eLU) function for the hidden layer of the pilot assignment branch, defined as

$$\text{eLU}(a_i) = \begin{cases} \Gamma\cdot(e^{a_i}-1), & \text{if } a_i < 0, \\ a_i, & \text{otherwise} \end{cases} \tag{26}$$

where Γ determines the function saturation point for the negative input values. The softmax function is used in all the output layers of the pilot assignment branch. In particular, the kth sub-branch activation is calculated as

$$v_{ki} = \text{softmax}(a_{ki}) = \frac{e^{a_{ki}}}{\sum_{i=1}^{P} e^{a_{ki}}} \tag{27}$$

where v_{ki} represents the ith element of vector $\boldsymbol{v}_k \in \mathbb{R}^{P\times 1}$. The softmax values are then mapped to the pilots as

$$w = \underset{i\in\{1,2,\ldots,P\}}{\arg\max}\ v_{ki} \tag{28a}$$

$$\hat{\boldsymbol{\phi}}_k = \boldsymbol{p}_w \tag{28b}$$

where $\boldsymbol{p}_w$ is the wth pilot sequence.

C. LOSS FUNCTION

Since the optimal power control and pilot assignment schemes are unknown, we lack the labels required for supervised training of the neural network. Therefore, we perform unsupervised training for the multi-task DNN using a custom loss function specifically designed to execute power control and pilot assignment tasks while simultaneously

limiting user energy consumption. The proposed custom loss function is

$$\mathcal{L}\left(\hat{\boldsymbol{b}}, \hat{\boldsymbol{q}}, \boldsymbol{\Theta}; \boldsymbol{\psi}\right) = \sum_{k=1}^{K} \sigma\left(\frac{0.3}{R_k}\right) - K\lambda_1 R_{\min} + \lambda_2 \sum_{k=1}^{K} \hat{q}_k + \lambda_3 \sum_{k=1}^{K} \hat{b}_k + \frac{2\lambda_4}{K-1} \sum_{i=1}^{K} \sum_{j=1}^{i-1} \frac{\Theta_{ij}}{e^{\Omega_{ij}}}. \quad (29)$$

where λ_1, λ_2, λ_3, and λ_4 are the weights of the loss terms, $\boldsymbol{\psi}$ is the vector containing all the DNN's weights and biases, and vectors $\hat{\boldsymbol{b}}$ and $\hat{\boldsymbol{q}}$ are the pilot and data power coefficients assigned to the users by the DNN. The loss function (29) does not explicitly depend on $\boldsymbol{\psi}$; rather, it depends on $\boldsymbol{\psi}$ indirectly through $\hat{\boldsymbol{b}}$ and $\hat{\boldsymbol{q}}$, which are the outputs of the DNN. The first two terms of the loss function lay the foundation of our approach, solving the max-min problem as outlined in [25]. The constant 0.3 is a hyperparameter that specifies the degree to which the network is penalized for low or high throughput rates. We have conducted extensive simulations varying the value of such constant from 0 to 1, finding that 0.3 provides the best overall performance, in accordance to [25]. We have further enhanced the joint pilot and data power control and pilot assignment optimization performance by incorporating three additional terms into the loss function. The normalized sum of the assigned data power coefficients, $\frac{1}{K}\sum_{k=1}^{K}\hat{q}_k$, penalizes the allocation of high data power coefficients to the users during the training process, reducing the overall network transmit power and potentially increasing the nodes battery life. Similarly, the normalized sum of the assigned pilot power coefficients, $\frac{1}{K}\sum_{k=1}^{K}\hat{b}_k$ penalizes the network to reduce the pilot transmit power. The last term of (29) promotes the reuse of pilots among users that are far apart in the network area, limiting inter-user interference. The penalty becomes significant when nearby users utilize the same pilot, while it is minimized when users, whether in close proximity or at a significant distance, are allocated distinct pilots. The matrix $\boldsymbol{\Theta} = \{\Theta_{ij}\}$ is defined as $\boldsymbol{\Theta} = \boldsymbol{V}\boldsymbol{V}^T$, where $\boldsymbol{V} = [\boldsymbol{v}_1, \boldsymbol{v}_2, \ldots, \boldsymbol{v}_K]^T \in \mathbb{R}^{K\times P}$. Here, $\boldsymbol{v}_k$ represents the output of the softmax operation (27) of the kth sub-branch of pilot assignment as shown in Fig. 2. The normalized distance between the ith and the jth users is denoted by Ω_{ij}, and is obtained dividing the actual distance by $D\sqrt{2}$, where D denotes the simulation area side. As matrix $\boldsymbol{\Omega}$ is symmetric, we consider the sum of the elements below the diagonal and divide the result by the number of entries, $(K^2-K)/2$. It is important to note that the distances between the nodes and the APs are used solely for neural network training. After the training phase, only the large-scale fading coefficients are required to perform power control and pilot assignment. To simplify the notation, the aforementioned terms are multiplied by K, and each term is assigned a specific weight. Such weights are designed to enhance the model's adaptability by prioritizing various aspects critical to specific applications, such as minimizing power consumption in low-power scenarios.

Algorithm 1 Training Algorithm of JPDCPA DNN

Input: $\boldsymbol{\chi}$, $\boldsymbol{\Theta}$, β_1, β_2, δ, ϵ
Initialization: $t \leftarrow 1$, $\boldsymbol{v}^0 \leftarrow 0$, $\boldsymbol{s}^0 \leftarrow 0$
1: Initialize $\boldsymbol{\psi}^t$
2: **while** parameters do not converge **do**
3: $\{\hat{\boldsymbol{b}}, \hat{\boldsymbol{q}}, \hat{\boldsymbol{\Phi}}\} \leftarrow \Upsilon(\boldsymbol{\chi}; \boldsymbol{\psi}^t)$
4: $\nabla\mathcal{L} \leftarrow \partial\mathcal{L}(\hat{\boldsymbol{b}}, \hat{\boldsymbol{q}}, \boldsymbol{\Theta}; \boldsymbol{\psi}^{t-1})/\partial\boldsymbol{\psi}^{t-1}$
5: $\boldsymbol{v}^t \leftarrow \beta_1\boldsymbol{v}^{t-1} + (1-\beta_1)\nabla\mathcal{L}$
6: $\boldsymbol{s}^t \leftarrow \beta_2\boldsymbol{s}^{t-1} + (1-\beta_2)\nabla\mathcal{L}^2$
7: $\hat{\boldsymbol{v}}^t \leftarrow \boldsymbol{v}^t/(1-\beta_1^t)$
8: $\hat{\boldsymbol{s}}^t \leftarrow \boldsymbol{s}^t/(1-\beta_2^t)$
9: $\boldsymbol{\psi}^t \leftarrow \boldsymbol{\psi}^{t-1} - \delta\hat{\boldsymbol{v}}^t/(\sqrt{\hat{\boldsymbol{s}}^t} + \epsilon)$
10: $t \leftarrow t+1$
11: **end while**
Return: $\boldsymbol{\psi}$

D. DNN TRAINING AND INFERENCE

The proposed JPDCPA DNN, depicted in Fig. 2, can be seen as a function that maps the pre-processed large-scale fading coefficients $\boldsymbol{\chi}$ to the data and pilot power control coefficients and the assigned pilots $\hat{\boldsymbol{b}}$, $\hat{\boldsymbol{q}}$, and $\hat{\boldsymbol{\Phi}} = [\hat{\boldsymbol{\phi}}_1, \hat{\boldsymbol{\phi}}_2, \ldots, \hat{\boldsymbol{\phi}}_K]^T$, using the learned weights $\boldsymbol{\psi}$, i.e.,

$$\{\hat{\boldsymbol{b}}, \hat{\boldsymbol{q}}, \hat{\boldsymbol{\Phi}}\} = \Upsilon(\boldsymbol{\chi}; \boldsymbol{\psi}). \quad (30)$$

In the training phase, the objective is to determine the optimal parameters that define the best mapping between the input and output. We begin by initializing the network parameters through He initialization [36]. Then, the network is fed with the input data, which are used to allocate the pilot and data power coefficients and to assign the pilots to the users. We use the Adam optimizer [37] to train the network. The steps for the Adam algorithm are outlined in Algorithm 1, lines 3-8, with β_1, β_2, the learning rate δ, and ϵ as hyperparameters. We optimize the network parameters until convergence, which is indicated by the absence of significant changes in the parameters values.

During inference, the network utilizes the weights and biases learned during training. We remark that, since there is no need to evaluate the loss function for parameter optimization during the inference stage, user location data is no longer required. At this point, the trained network can operate in real-time, performing pilot and data coefficient allocation and pilot assignment based on the current pre-processed large-scale fading coefficients of the network users.

VI. NUMERICAL RESULTS

This section describes the simulation setup and numerical results for the DL-based approach.

A. SIMULATION SETUP

Simulations are conducted for two distinct scenarios: a UMa scenario and an industrial one. Both scenarios have identical simulation area size and nodes and AP distributions.

The network area is a square of side $D = 1000$ m. For each sample of the dataset, the positions of the users are generated randomly and a different realization of the large-scale fading coefficients is considered. We consider four simulation settings with different numbers of APs, users, and orthogonal pilot sequences, namely: 1) $M = 64$, $K = 32$, $P = 10$ 2) $M = 121$, $K = 60$, $P = 20$, 3) $M = 64$, $K = 250$, $P = 24$, 4) $M = 64$, $K = 250$, $P = 24$. In all the simulation settings, the number of orthogonal pilot sequences is lower than the number of users. Furthermore, the first two settings illustrate situations where the number of users is less than the number of antennas, whereas in the last two simulation settings, the number of users exceeds the number of APs. The channel models adopted in the two scenarios are detailed below.

1) UMA SCENARIO

We adopt Hata-COST231 propagation model as in [4], with path-loss

$$\mathrm{PL}_{mk}[\mathrm{dB}] = \begin{cases} L + 35\log_{10} d_{mk}^{\mathrm{UM}}, \text{ if } d_{mk}^{\mathrm{UM}} > d_1 \\ L + 15\log_{10} d_1 + 20\log_{10} d_{mk}^{\mathrm{UM}}, \text{ if } d_0 < d_{mk}^{\mathrm{UM}} \leq d_1 \\ L + 15\log_{10} d_1 + 20\log_{10} d_0, \text{ if } d_{mk}^{\mathrm{UM}} < d_0 \end{cases} \quad (31)$$

where

$$L = 46.3 + 33.9\log_{10} f^{\mathrm{UM}} - 13.82\log_{10} h_{\mathrm{AP}} - \left(1.1\log_{10} f^{\mathrm{UM}} - 0.7\right)h_{\mathrm{u}} + \left(1.56\log_{10} f^{\mathrm{UM}} - 0.8\right)$$

and where f^{UM} is the carrier frequency in MHz, d_{mk}^{UM} is the distance between the kth device and mth AP in kilometers, d_0 and d_1 are the threshold distances associated with the path-loss model in kilometers, h_{AP} is the AP antenna height in meters, and h_{u} is the device antenna height in meters.

2) INDUSTRIAL SCENARIO

We consider an indoor industrial scenario with the following path-loss model [33]

$$\mathrm{PL}_{mk}[\mathrm{dB}] = +32.40 + 23\log_{10} d_{mk}^{\mathrm{IN}} + 20\log_{10} f^{\mathrm{IN}}. \quad (32)$$

where f^{IN} is the carrier frequency in GHz and d_{mk}^{IN} is the distance between the mth AP and kth user in meters. The complete list of simulation parameters is reported in Table 1.

A set consisting of 5×10^4 and 10^3 different samples are used for training and testing the multi-task DNN model, respectively. We initialize the network with He initialization [36]. The network is trained using mini-batches of 100 samples for 30 epochs adopting the Adam optimizer [37]. The initial learning rate δ is set to 0.01, which is updated after each epoch using $\delta_i = \delta_{i-1}e^{-0.1}$, where i represents the ith epoch. We have allocated the same weight to each term, reflecting equal importance to spectral efficiency, power allocation, and pilot assignment, i.e., $\lambda_1 = \lambda_2 = \lambda_3 = \lambda_4 = 1$. The eLU saturation parameter Γ is set to 0.2.

TABLE 1. Simulation parameters.

Parameters	Value
Simulation settings	$M = 64$, $K = 32$, $P = 10$, $M = 121$, $K = 60$, $P = 20$, $M = 64$, $K = 250$, $P = 24$, $M = 121$, $K = 500$, $P = 48$.
Transmit power ($\bar{\rho}_{\mathrm{p}}$, $\bar{\rho}$)	100 mW
Bandwidth (B)	20 MHz
Noise figure (NF)	9 dB
Noise temperature (T_0)	290 K
Packet length (τ_{c})	400
Urban Macro scenario	
Pathloss model	Defined in (31)
Carrier frequency (f^{UM})	1.9 GHz
Shadowing coefficient ($\sigma_{\mathrm{sh}}^{\mathrm{UM}}$)	8 dB
Height of AP antenna (h_{AP})	15 m
Height of user antenna (h_{u})	1.65 m
Path-loss model d_0, d_1	10 m, 50 m
Industrial scenario	
Pathloss model	Defined in (32)
Carrier frequency (f^{IN})	1.9 GHz
Shadowing coefficient ($\sigma_{\mathrm{sh}}^{\mathrm{IN}}$)	5.9 dB

B. PERFORMANCE METRICS

The performance metrics considered in this section are per-user network uplink throughput rate and minimum user rate, defined as [4]

$$R_k^{\mathrm{net}} = \frac{\tau_{\mathrm{d}}}{\tau_{\mathrm{c}}} B R_k \quad (33)$$

and

$$R_k^{\mathrm{min}} = \frac{\tau_{\mathrm{d}}}{\tau_{\mathrm{c}}} \min_k R_k \quad (34)$$

respectively, where $\tau_{\mathrm{d}} = \tau_{\mathrm{c}} - \tau$ is the data payload length. We compare three algorithms to our approach: random assignment (RA), joint power control and pilot assignment (JPCPA), and deep learning power control (DLPC). The minimum user rate serves as an appropriate performance indicator for user fairness, ensuring quality service for all users. In the RA algorithm, we allocate equal power to all users, ensuring that the total transmit power matches our DL approach, and assign pilots randomly. For instance, if JPDCPA distributes 10 mW among 10 users, RA algorithm assigns 1 mW to each user. In JPCPA, the focus is on optimizing data power allocation and pilot assignment. We employ the architecture depicted in Fig. 2 with the omission of the pilot power allocation branch. The network is trained for 30 epochs utilizing the loss function (29) with $\lambda_1 = \lambda_2 = \lambda_4 = 1$ and $\lambda_3 = 0$. Conversely, DLPC is a two-stage algorithm that combines two state-of-the-art methods and works as follows. First, the pilot assignment is performed using the strategy proposed in

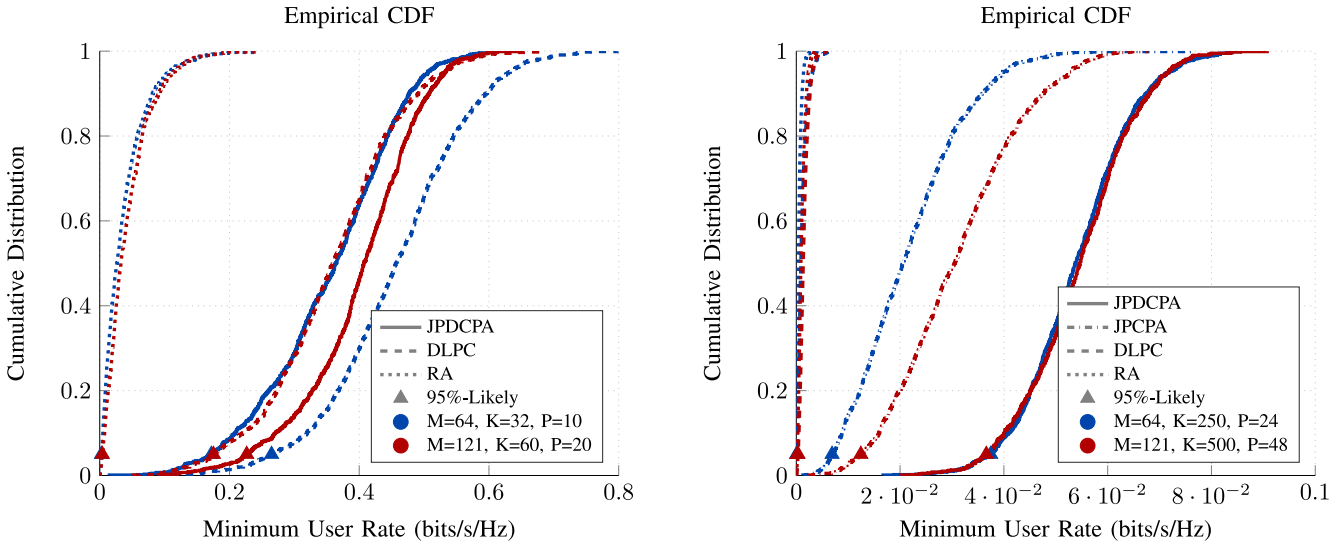

(a) The number of APs exceeds the number of users.

(b) The number of users exceeds the number of APs.

FIGURE 3. Cumulative distribution of minimum user rate in the UMa scenario with $N = 1$.

[38, Algorithm 4.1] [17]. Then, we obtain power coefficients through the DNN proposed in [25], which is designed to optimize power control when the number of active users is less than that of the APs.

C. MINIMUM USER RATE

Fig 3 shows the cumulative distribution of minimum user rate in the UMa scenario. Specifically, Fig. 3(a) shows the results for the scenario where the number of APs exceeds the number of users. It can be observed that, with $M = 64$ and $K = 32$, DLPC yields the best performance, whereas RA exhibits the worst performance. Specifically, for $M = 64$ and $K = 32$, RA, DLPC, and JPDCPA achieve 95%-likely minimum user rates of 0.004, 0.2648, and 0.1719 bits/s/Hz, respectively. However, for $M = 121$ and $K = 60$, JPDCPA outperforms the other approaches yielding 0.2265 bits/s/Hz 95%-likely minimum user rate. Furthermore, the performance of DLPC decreases considerably as the scenario size increases, indicating a scalability issue.

The plot in Fig. 3(b) clearly indicates a substantial increase in the minimum user rate in JPDCPA compared to other approaches in the UMa scenario. Specifically, when the number of users exceeds that of the APs, DLPC exhibits limited performance, yielding only marginal improvements compared to RA. The JPCPA model achieves a lower median value of 0.019 bits/s/Hz for the minimum user rate on the test set compared to 0.055 bits/s/Hz through JPDCPA with $M = 64, K = 250$. The median of the empirical cumulative distribution function (CDF) of minimum user rate exhibited a substantial increase of approximately 56% from the simulation scenario with $M = 64, K = 250$ to $M = 121$, $K = 500$ with JPCPA. In contrast, with JPDCPA, the curves overlap, with the performance for $M = 121, K = 500$ showing a marginal improvement compared to $M = 64$, $K = 250$.

To demonstrate the adaptability of our approach, we tested the proposed multi-task DNN in the industrial scenario with $M = 64$ and $M = 121$ configuration. The empirical CDF for the minimum user rate is depicted in Fig. 4(a), where the number of APs exceeds the number of users. DLPC outperforms the other approaches when $M = 64$ and $K = 32$. Conversely, for $M = 121$ and $K = 60$, JPDCPA outperforms both DLPC and RA. Precisely, JPDCPA provides 0.2652 bit/s/Hz, whereas DLPC and RA results in 0.1818 and 0.0043 bit/s/Hz 95%-likely minimum user rate, respectively.

The minimum user rate in the industrial scenario where the number of users exceeds the number of APs is illustrated in Fig. 4(b). It is evident from the figure that the JPDCPA outperforms the baseline approaches considerably. Specifically, in a simulation setting with $M = 64, K = 250$ and $M = 121, K = 500$, JPDCPA exhibits an increase of 157% and 89% in the of 95%-likely throughput rate from JPCPA, respectively. The JPDCPA performs slightly better in a smaller scenario, i.e., $M = 64, K = 250$, showing an opposite behavior compared to the UMa scenario. This discrepancy arises due to the difference in the path-loss models and large-scale fading intensities between the two scenarios. In UMa scenario, the channel is more selective in space, which decreases interference and slightly boosts performance in $M = 121$ compared to $M = 64$.

In Fig 5, we report the minimum user rate when considering multiple antennas APs for JPDCPA, DLPC, and RA algorithms. It can be observed that increasing the number of antennas at each AP yields tangible improvements in minimum user rates for all algorithms. Specifically, for JPDCPA we observe an increase in the 95%-likely throughput rate, escalating from 0.036 bits/s/Hz (for $N = 1$) to 0.14 bits/s/Hz (for $N = 4$) and 0.26 bits/s/Hz (for $N = 8$). Furthermore, in terms of the median value of the minimum

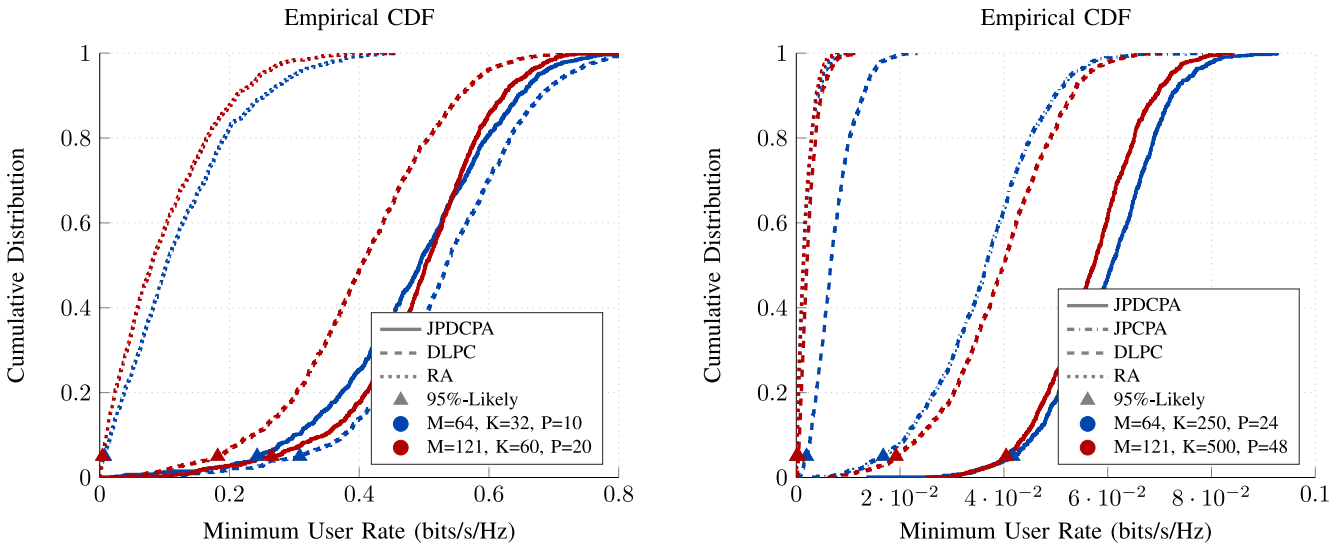

(a) The number of APs exceeds the number of users.

(b) The number of users exceeds the number of APs.

FIGURE 4. Cumulative distribution of minimum user rate in the industrial scenario with $N = 1$.

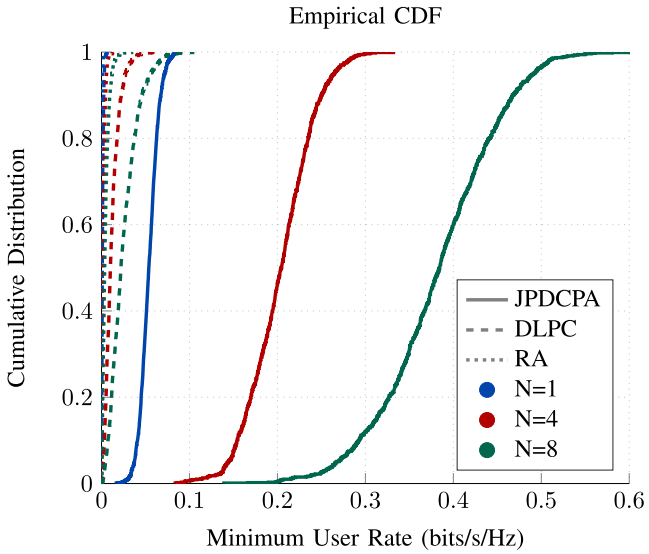

FIGURE 5. Cumulative distribution of minimum user rate in the UMa scenario with $M = 64$, $K = 250$, $P = 24$, considering multiple antennas at the APs.

user rate, JPDCPA with $N = 1$ antenna yields five times better performance than the DLPC with $N = 1$.

D. PER-USER UPLINK NET THROUGHPUT

The empirical CDFs for the per-user uplink throughput rate in a UMa scenario for configurations with $M = 121$, $K = 60$ is depicted in Fig. 6(a). In this configuration, JPDCPA, JPCPA, and DLPC exhibit similar performance in the lower region of the curves, but DLPC takes the lead in the upper region. More precisely, in terms of the median value of the per-user uplink throughput rate, DLPC shows an increase of 9.54% and 15.17% over JPCPA and JPDCPA, respectively.

In the simulation setting with $M = 64, K = 250$ as depicted in Fig. 6(b), our approach yields a significantly higher 95%-likely per-user net uplink throughput rate of 1.89 Mbits/s. In contrast, RA and DLPC attain only 0.08 Mbits/s and 0.21 Mbits/s, respectively. Furthermore, JPDCPA aligns with the trajectory of JPCPA, exhibiting a slight improvement in the lower region of the curve in both scenarios. For the simulation setting with $M = 64$, $K = 250$ depicted in Fig. 6(b), JPDCPA observe an increase of 20% in the 95%-likely per-user net throughput with respect to JPCPA. Similarly, 8% increment in 95%-likely per-user net throughput with respect to JPCPA can be observed in Fig. 6(c).

The per-user uplink throughput in the industrial scenario where the numbers of APs exceed the number of users is depicted in Fig. 7(a). It can be observed that DLPC, JPCPA, and JPDCPA exhibit similar performance, whereas RA demonstrates the worst performance. More precisely, JPDCPA, JPCPA, and DLPC show median values of 20.16 Mbits/s for the empirical CDF of the per-user net throughput rate in $M = 121, K = 60$ scenario. Conversely, Fig. 7(b) and Fig. 7(c) show the curves for the scenario, where the number of users exceeds the number of APs. Notably, JPDCPA exhibits 1.19 Mbits/s and 2.06 Mbits/s 95%-likely per-user uplink throughput rate in $M = 64, K = 250$ and $M = 121$, $K = 500$ scenarios, respectively. Moreover, the median of the empirical CDF of the per-user uplink throughput rate in JPDCPA is 1.21 and 1.38 times that of the DLPC in $M = 64$, $K = 250$ and $M = 121, K = 500$, respectively. JPDCPA demonstrates a slight improvement over JPCPA in terms of both 95%-likely and median of the empirical CDF. For instance, with $M = 64, K = 250$, JPCPA achieves 1.59 Mbits/s, whereas JPDCPA obtains 1.92 Mbits/s 95%-likely per-user uplink throughput rate.

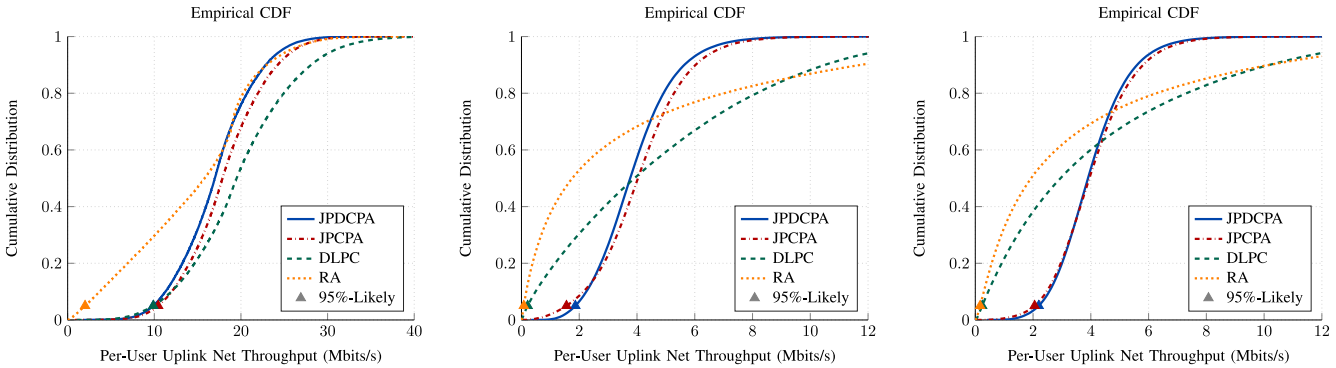

(a) $M = 121$, $K = 60$, $P = 20$. (b) $M = 64$, $K = 250$, $P = 24$. (c) $M = 121$, $K = 500$, $P = 48$.

FIGURE 6. Cumulative distribution of per-user net throughput in the UMa scenario with $N = 1$.

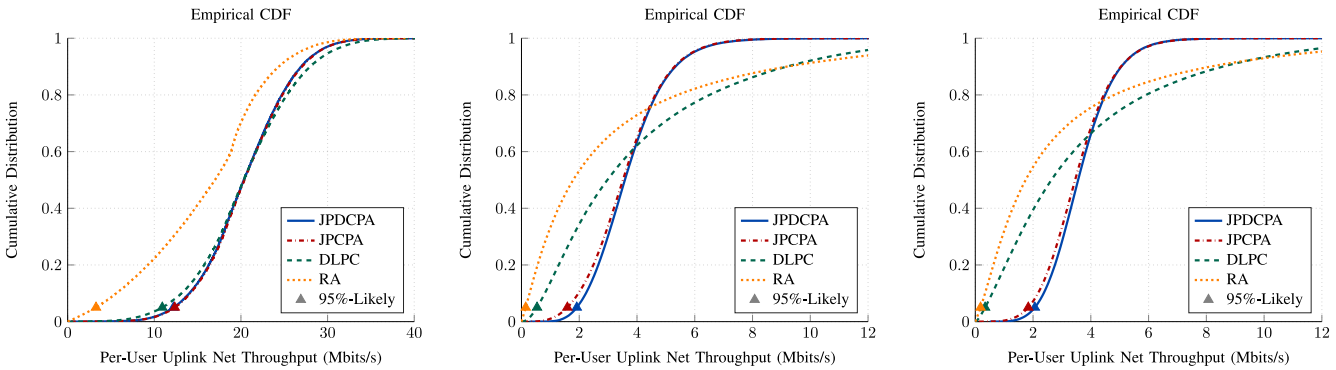

(a) $M = 121$, $K = 60$, $P = 20$. (b) $M = 64$, $K = 250$, $P = 24$. (c) $M = 121$, $K = 500$, $P = 48$.

FIGURE 7. Cumulative distribution of per-user net throughput in an industrial scenario with $N = 1$.

E. PER-USER POWER USAGE

To demonstrate the advantage of the proposed method in terms of energy efficiency, we compute the average per-user pilot and data transmit powers as

$$P_{\mathrm{C}}^{\mathrm{p}} = \frac{\bar{\rho}_{\mathrm{p}}}{KS} \sum_{i=1}^{S} \sum_{k=1}^{K} \hat{b}_{k,i} \tag{35}$$

and

$$P_{\mathrm{C}} = \frac{\bar{\rho}}{KS} \sum_{i=1}^{S} \sum_{k=1}^{K} \hat{q}_{k,i} \tag{36}$$

respectively. Here, S represents the number of test samples. The result of this analysis is shown in Table 2. DLPC and JPCPA transmit the pilot with maximum power, resulting in an average per-user power usage of 20 dBm. In contrast, JPDCPA includes the term $\sum_{k=1}^{K} \hat{b}_k$ in the loss function, that penalizes the network for high power allocation for pilot transmission. Consequently, JPDCPA yields the lowest average per-user pilot transmit power.

Regarding data transmit power, DLPC shows the highest consumption as its loss function lacks a penalty term for high data transmission power. On the other hand, both JPCPA and JPDCPA incorporate the term $\sum_{k=1}^{K} \hat{q}_k$ in the loss function to penalize high data power allocation. Specifically, for $M = 121$, $K = 500$ in the UMa scenario, DLPC results in 16.81 dBm per-user data power consumption, while JPCPA and JPDCPA achieve significantly lower power consumption of 1.58 dBm and 1.64 dBm, respectively. Furthermore, JPDCPA has the lowest data transmit power for $M = 64, K = 32$ and $M = 121, K = 60$ scenarios. However, JPCPA yields the lowest power consumption for data transmission for $M = 64, K = 250$ and $M = 121, K = 500$ scenarios. Nevertheless, considering both pilot and data transmit power, JPDCPA provides the least power consumption overall.

It is noteworthy that for JPCPA and JPDCPA, the data transmit power increases as the number of APs decreases. Specifically, in both UMa and industrial scenarios, the data transmit power for the $M = 121, K = 60$ ($M = 121, K = 500$) scenario is lower than that for the $M = 64, K = 32$ ($M = 64, K = 250$) scenario, respectively. A similar trend is observed for JPDCPA and JPCPA in terms of pilot transmit power. This is because, with an increase in the number of APs, users are in proximity to the APs, which allows them to transmit with less power compared to the scenario with lower AP density, where the distance between APs and the user is greater. Furthermore, in the UMa scenario, JPDCPA exhibits lower pilot transmit power in comparison to data transmit power.

TABLE 2. Average per-user transmit power in dBm.

	Pilot Transmit Power (P_C^p)			Data Transmit Power (P_C)			
	DLPC [17], [25]	JPCPA	JPDCPA	DLPC	JPCPA	JPDCPA	
$M = 64,\ K = 32,\ P = 10$	20.00	20.00	5.9765	13.81	7.1749	7.0642	UMa
$M = 121,\ K = 60,\ P = 20$	20.00	20.00	3.5086	13.92	4.9933	4.8997	
$M = 64,\ K = 250,\ P = 24$	20.00	20.00	2.5243	15.02	3.5386	3.8467	
$M = 121,\ K = 500,\ P = 48$	20.00	20.00	0.1417	16.81	1.5828	1.6378	
$M = 64,\ K = 32,\ P = 10$	20.00	20.00	−1.5196	13.25	−2.3937	−2.4794	Industrial
$M = 121,\ K = 60,\ P = 20$	20.00	20.00	−3.4917	16.37	−4.2163	−4.2575	
$M = 64,\ K = 250,\ P = 24$	20.00	20.00	−6.7493	18.68	−6.6161	−6.4878	
$M = 121,\ K = 500,\ P = 48$	20.00	20.00	−8.5374	17.77	−8.2732	−8.0644	

TABLE 3. Average per-user transmit power (dBm) in UMa scenario, with and without the third and fourth loss function terms.

	Pilot Transmit Power		Data Transmit Power	
	No PC	PC	No PC	PC
$M = 64,\ K = 32$	17.47	5.9765	11.57	7.0642
$M = 121,\ K = 60$	17.55	3.5086	10.37	4.8997
$M = 64,\ K = 250$	12.04	2.5243	9.5368	3.8467
$M = 121,\ K = 500$	12.83	0.1417	8.7085	1.6378

F. LOSS FUNCTION EVALUATION

The proposed loss function (29) is specifically designed to address the max-min problem (18); however, the third and fourth terms of (29) are intended to penalize the allocation of high per-user data and pilot transmit power, respectively. We perform a comparative analysis to assess the benefits provided by these terms. Specifically, we evaluate the pilot and data transmit power after training the DNN with and without the third and fourth terms in the considered UMa scenario. The results of this analysis are provided in Table 3, where "PC" indicates the inclusion of these terms, and "No PC" indicates their exclusion from the loss function. The table clearly shows that introducing the power control terms significantly reduces network power utilization. Precisely, for $M = 64, K = 500$, the pilot and data transmit powers are reduced by a factor of 90.54 and 5.32, respectively. The data transmit power decreases as the scenario size increases. For instance, the data transmit power decreases from 11.57 dBm to 8.71 dBm when moving from $M = 64, K = 32$ to $M = 121,\ K = 500$.

The last term of the loss function aims to minimize inter-user interference by discouraging the assignment of identical pilots to users who are located near each other. To assess the performance improvement resulting from the addition of the last term to the proposed loss function, we have conducted a comparative evaluation. We have trained the network with only the first four terms in (29), and compared it to the model trained considering all five terms. In Fig. 8, we present the CDFs for the minimum user rate for $M = 64$ and $M = 121$ in the UMa scenario. It can be observed that incorporating the last term yields a gain of $5 - 6\%$ in the median value of the minimum user rate. Similarly, an increase of $7 - 9\%$ can be seen in the minimum user rate at the 95% likelihood threshold.

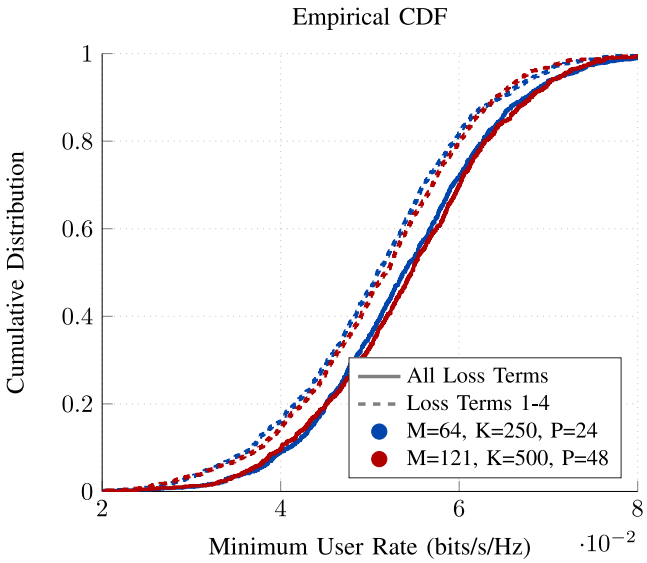

FIGURE 8. Cumulative distribution of the minimum user rate in the considered UMa scenario. Performance comparison between the DNN trained using the first four loss terms and the DNN trained using all loss terms.

G. COMPUTATIONAL COMPLEXITY

The computational complexity of the algorithms is evaluated in terms of FLOPs. The real addition, subtraction, and multiplication, are taken as a single FLOP while division and exponential operations as 4 and 8 FLOPs, respectively [39]. The operations argmax($\boldsymbol{v}$) and argmin($\boldsymbol{v}$) applied to vector $\boldsymbol{v}$ of length V are assumed to require $V - 1$ FLOPs.

1) JPDCPA

The computational complexities of the pilot power allocation, data power allocation, and pilot assignment branches are analyzed separately. The total complexity is then calculated by summing the individual contributions.

Pilot Power Allocation: The computational complexity of the fully-connected layer in terms of FLOPs can be calculated as

$$C_{\text{FC}}^{\text{PP}} = 2K^2.$$

The sigmoid function requires 13 FLOPs for each evaluation. As the sigmoid function is evaluated K times, the total number of FLOPs required is $13K$. Thus, the total computational complexity of the pilot power allocation branch is

$$C_{\text{tot}}^{\text{PP}} = 2K^2 + 13K. \tag{37}$$

Data Power Allocation: Following the same methodology used for pilot power allocation branch, the overall computational complexity of the data power allocation branch is

$$C_{\text{tot}}^{\text{DP}} = 2K^2 + 13K. \tag{38}$$

Pilot Assignment: The computational complexity of the first fully-connected layer of the pilot assignment branch is

$$C_{\text{FC}_1}^{\text{PA}} = 20K.$$

This layer utilizes the eLU activation function. For negative inputs, the computational cost is 10 FLOPs, whereas it is 1 FLOP for positive inputs. Considering the worst-case scenario, we can assume a cost of 10 FLOPs per eLU operation. Considering that the eLU operation is executed 10 times, the overall complexity of the activation layer is

$$C_{\text{eLU}}^{\text{PA}} = 10 \cdot 10 = 100.$$

The pilot assignment branch is then divided into K sub-branches. The cumulative computational complexity of K fully-connected layers is

$$C_{\text{FC}_2}^{\text{PA}} = 20PK.$$

The softmax layer consists of P exponentials, $P-1$ summations, and P divisions. Following the softmax operation, we need to determine the maximum value of vector $\boldsymbol{\nu}_k$, which involves $P-1$ FLOPs. These two operations are iterated K times, corresponding to the number of sub-branches, contributing to the overall computational complexity

$$C_{\text{softmax}}^{\text{PA}} = 14PK - 2K.$$

Therefore, the total computational complexity of the pilot assignment branch is

$$\begin{aligned} C_{\text{tot}}^{\text{PA}} &= C_{\text{FC}_1}^{\text{PA}} + C_{\text{eLU}}^{\text{PA}} + C_{\text{FC}_2}^{\text{PA}} + C_{\text{softmax}}^{\text{PA}} \\ &= 34PK + 18K + 100. \end{aligned} \tag{39}$$

2) TOTAL COMPUTATIONAL COMPLEXITY

The total computational complexity of the JPDCPA is

$$\begin{aligned} C_{\text{tot}} &= C_{\text{tot}}^{\text{PP}} + C_{\text{tot}}^{\text{PD}} + C_{\text{tot}}^{\text{PA}} \\ &= 4K^2 + 44K + 34PK + 100. \end{aligned} \tag{40}$$

TABLE 4. Computational cost in FLOPs.

	DLPC	JPCPA	JPDCPA
$M = 64,\ K = 32$	1.50×10^5	1.40×10^4	1.65×10^4
$M = 121,\ K = 60$	1.69×10^5	5.00×10^4	5.79×10^4
$M = 64,\ K = 250$	2.83×10^5	3.37×10^5	4.65×10^5
$M = 121,\ K = 500$	4.72×10^5	1.33×10^6	1.84×10^6

3) JPCPA

The JPCPA follows the same architecture as the JPDCPA, with the omission of the pilot power assignment branch. Thus, the computational complexity is

$$\begin{aligned} C_{\text{tot}} &= C_{\text{tot}}^{\text{PD}} + C_{\text{tot}}^{\text{PA}} \\ &= 2K^2 + 31K + 34PK + 100. \end{aligned} \tag{41}$$

4) DLPC

The pilot assignment algorithm consists of two stages. In the first stage, each pilot is randomly assigned to a user, with a complexity of P FLOPs. In the second stage, each of the remaining users identifies the AP with which it has the strongest channel, requiring $(M-1)(K-P)$ FLOPs. Subsequently, each remaining user calculates, for each pilot, the sum of the average channel gains towards the selected AP of the users already assigned to that pilot. The pilot that results in the lowest sum interference is then assigned to the respective user. Assuming that the already calculated sums are stored in memory and do not need to be recalculated, this process requires $K(P-1)$ FLOPs. Thus, the overall complexity is:

$$C_{\text{tot}}^{\text{PA}} = M(K-P) + K(P-2) + 2P. \tag{42}$$

Considering the proposed network architecture, the total computational complexity of data power allocation through the DNN [25] is

$$C_{\text{tot}}^{\text{DP}} = 525K + 131584.$$

Thus, the total computational complexity of DLPC is

$$C_{\text{tot}} = M(K-P) + K(P+523) + 2P + 131584. \tag{43}$$

The computational complexities for JPDCPA, JPCPA, and DLPC are presented in Table 4. The computational complexities of the algorithms increase with the scenario size. The table clearly shows that DLPC offers highest computational complexity for settings $M = 64, K = 32$ and $M = 121, K = 60$ while the lowest computational complexity for the settings $M = 64, K = 250$ and $M = 121$, $K = 500$. This suggests that the JPCPA and JPDCPA are more significantly impacted by an increase in the number of users and pilots compared to DLPC. For instance, for the $M = 121, K = 60$ scenario, the complexity of DLPC is 9.1 times that of JPDCPA, whereas, for the $M = 121, K = 500$ scenario, the complexity of JPDCPA is 3.9 times that of DLPC. Including the pilot power control branch in JPDCPA results in $2K^2 + 13K$ more FLOPs than JPCPA.

VII. CONCLUSION

In this paper, we proposed a scalable multi-task DNN-based solution called JPDCPA for joint pilot and data power allocation and pilot assignment in CF-mMIMO scenarios. We considered a massive access scenario where the number of users exceeds the available orthogonal pilots. The adaptability of JPDCPA is demonstrated by assessing its performance in a UMa and indoor industrial scenarios. Numerical results show that the proposed multi-task DNN effectively addresses the joint power control and pilot allocation problem, surpassing a state-of-the-art approach in terms of both achievable network throughput and minimum user rate. Furthermore, the unsupervised training of the JPDCPA using the proposed loss function not only outperforms alternative methods in enhancing users' spectral efficiency but also leads to a significant reduction in average transmit power per user compared to the considered state-of-the-art solution.

APPENDIX

To derive the closed-form expression for the achievable rate given in (19), we need to compute DS_k, $\mathbb{E}\{|\mathrm{BU}_k|^2\}$, $\mathbb{E}\{|\mathrm{IUI}_{kk'}|^2\}$, and $\mathbb{E}\{|\mathrm{TN}_k|^2\}$.

A. COMPUTE DS_K

The term DS_k can be expressed as [4], [15]

$$\mathrm{DS}_k = \sqrt{\rho q_k} N \sum_{m=1}^{M} \gamma_{mk}. \tag{44}$$

B. COMPUTE $\mathbb{E}\{|\mathrm{BU}_K|^2\}$

The expression, following the derivation outlined in [4], [15], is

$$\mathbb{E}\{|\mathrm{BU}_k|^2\} = \rho N \sum_{m=1}^{M} q_k \gamma_{mk} \beta_{mk} \tag{45}$$

C. COMPUTE $\mathbb{E}\{|\mathrm{IUI}_{KK'}|^2\}$

The term can be calculated as

$$\mathbb{E}\{|\mathrm{IUI}_{kk'}|^2\} = \rho \mathbb{E}\left\{ \left| \sum_{m=1}^{M} \sum_{n=1}^{N} \hat{g}_{mnk}^{*} g_{mnk'} \sqrt{q_{k'}} \right|^2 \right\}.$$

Substituting $\hat{g}_{mnk}^{*} = c_{mk} \tilde{y}_{mnk}^{*}$ yields to (46), shown at the bottom of the page. Since $\tilde{w}_{mn} = \boldsymbol{\phi}_k^H \boldsymbol{w}_{mn} \sim \mathcal{CN}(0, 1)$ is independent of g_{mnk}, the term A is

$$A = \rho q_{k'} N \sum_{m=1}^{M} c_{mk}^2 \beta_{mk'}.$$

Recalling that $\mathbb{E}\{|X+Y|^2\} = \mathbb{E}\{|X|^2\} + \mathbb{E}\{|Y|^2\}$ where X and Y are two independent random variables and $\mathbb{E}\{X\} = 0$, B can be expressed as in (47), shown at the bottom of the page. Manipulating B1 we obtain (48), shown at the top of the next page. Manipulating B2 yields (49), shown at the top of the next page. By incorporating the expressions for A, $B1$, and $B2$ into (46) we obtain

$$\mathbb{E}\{|\mathrm{IUI}_{kk'}|^2\} = \rho q_{k'} |\boldsymbol{\phi}_k^H \boldsymbol{\phi}_{k'}|^2 N \left(\sum_{m=1}^{M} \gamma_{mk} \frac{\sqrt{b_{k'}} \beta_{mk'}}{\sqrt{b_k} \beta_{mk}} \right)^2 + \rho q_{k'} N \sum_{m=1}^{M} \gamma_{mk} \beta_{mk'}. \tag{50}$$

D. COMPUTING $\mathbb{E}\{|\mathrm{TN}_K|^2\}$

$$\mathbb{E}\{|\mathrm{TN}_k|^2\} = \mathbb{E}\left\{ \left| \sum_{m=1}^{M} \sum_{n=1}^{N} \hat{g}_{mnk}^{*} \nu_{mn} \right|^2 \right\} = N \sum_{m=1}^{M} \gamma_{mk}. \tag{51}$$

Substituting (44), (45), (50), (51) into (16) yields (19).

$$\begin{aligned} \mathbb{E}\{|\mathrm{IUI}_{kk'}|^2\} &= \rho \mathbb{E}\left\{ \left| \sum_{m=1}^{M} \sum_{n=1}^{N} c_{mk} g_{mnk'} \sqrt{q_{k'}} \left(\sqrt{\tau \rho_{\mathrm{p}}} \sum_{i=1}^{K} \sqrt{b_i} g_{mni} \boldsymbol{\phi}_k^H \boldsymbol{\phi}_i + \boldsymbol{\phi}_k^H \boldsymbol{w}_{mn} \right)^* \right|^2 \right\} \\ &= \underbrace{\rho q_{k'} \mathbb{E}\left\{ \left| \sum_{m=1}^{M} \sum_{n=1}^{N} c_{mk} g_{mnk'} \left(\boldsymbol{\phi}_k^H \boldsymbol{w}_{mn} \right)^* \right|^2 \right\}}_{A} + \underbrace{\tau \rho_{\mathrm{p}} \rho \mathbb{E}\left\{ \left| \sum_{m=1}^{M} \sum_{n=1}^{N} \sqrt{q_{k'}} c_{mk} g_{mnk'} \left(\sum_{i=1}^{K} \sqrt{b_i} g_{mni} \boldsymbol{\phi}_k^H \boldsymbol{\phi}_i \right)^* \right|^2 \right\}}_{B}. \end{aligned} \tag{46}$$

$$B = \underbrace{\tau \rho_{\mathrm{p}} \rho \, \mathbb{E}\left\{ \left| \sum_{m=1}^{M} \sum_{n=1}^{N} \sqrt{q_{k'}} c_{mk} g_{mnk'} \left(\sqrt{b_{k'}} g_{mnk'} \boldsymbol{\phi}_k^H \boldsymbol{\phi}_{k'} \right)^* \right|^2 \right\}}_{B1} + \underbrace{\tau \rho_{\mathrm{p}} \rho \, \mathbb{E}\left\{ \left| \sum_{m=1}^{M} \sum_{n=1}^{N} \sqrt{q_{k'}} c_{mk} g_{mnk'} \left(\sum_{i \neq k'}^{K} \sqrt{b_i} g_{mni} \boldsymbol{\phi}_k^H \boldsymbol{\phi}_i \right)^* \right|^2 \right\}}_{B2}. \tag{47}$$

$$
\begin{aligned}
B1 &= \tau\rho_{\mathrm{p}}\rho\mathbb{E}\left\{\left|\sum_{m=1}^{M}\sum_{n=1}^{N}\sqrt{q_{k'}}c_{mk}g_{mnk'}\left(\sqrt{b_{k'}}g_{mnk'}\boldsymbol{\phi}_k^H\boldsymbol{\phi}_{k'}\right)^*\right|^2\right\} \\
&= \tau\rho_{\mathrm{p}}\rho b_{k'}q_{k'}|\boldsymbol{\phi}_k^H\boldsymbol{\phi}_{k'}|^2\mathbb{E}\left\{\sum_{m=1}^{M}\sum_{n=1}^{N}c_{mk}|g_{mnk'}|^2\sum_{t=1}^{M}\sum_{n=1}^{N}c_{tk}|g_{tnk'}|^2\right\} \\
&= \tau\rho_{\mathrm{p}}\rho b_{k'}q_{k'}|\boldsymbol{\phi}_k^H\boldsymbol{\phi}_{k'}|^2\mathbb{E}\left\{\sum_{m=1}^{M}\sum_{n=1}^{N}c_{mk}^2|g_{mnk'}|^4\right\} + \tau\rho_{\mathrm{p}}\rho b_{k'}q_{k'}|\boldsymbol{\phi}_k^H\boldsymbol{\phi}_{k'}|^2\sum_{m=1}^{M}\sum_{t\neq m}^{M}\sum_{n=1}^{N}c_{mk}c_{tnk}\beta_{mk'}\beta_{tk'} \\
&= \tau\rho_{\mathrm{p}}\rho b_{k'}q_{k'}|\boldsymbol{\phi}_k^H\boldsymbol{\phi}_{k'}|^2N\sum_{m=1}^{M}c_{mk}^2\beta_{mk'}^2 + \rho q_{k'}|\boldsymbol{\phi}_k^H\boldsymbol{\phi}_{k'}|^2N\left(\sum_{m=1}^{M}\gamma_{mk}\frac{\sqrt{b_{k'}}\beta_{mk'}}{\sqrt{b_k}\beta_{mk}}\right)^2. \qquad (48)
\end{aligned}
$$

$$
\begin{aligned}
B2 &= \tau\rho_{\mathrm{p}}\rho\mathbb{E}\left\{\sum_{m=1}^{M}\sum_{n=1}^{N}\sum_{i\neq k'}^{K}q_{k'}b_ic_{mk}^2|g_{mnk'}|^2|g_{mni}|^2|\boldsymbol{\phi}_k^H\boldsymbol{\phi}_i|^2\right\} \\
&= \tau\rho_{\mathrm{p}}\rho N\sum_{m=1}^{M}\sum_{i=1}^{K}q_{k'}b_ic_{mk}^2\beta_{mk'}\beta_{mi}|\boldsymbol{\phi}_k^H\boldsymbol{\phi}_i|^2 - \tau\rho_{\mathrm{p}}\rho N\sum_{m=1}^{M}q_{k'}b_{k'}c_{mk}^2\beta_{mk'}^2|\boldsymbol{\phi}_k^H\boldsymbol{\phi}_{k'}|^2 \\
&= \rho q_{k'}N\sum_{m=1}^{M}c_{mk}^2\beta_{mk'}\left(\tau\rho_{\mathrm{p}}\sum_{i=1}^{K}b_i\beta_{mi}|\boldsymbol{\phi}_k^H\boldsymbol{\phi}_i|^2 + 1\right) - \tau\rho_{\mathrm{p}}\rho N\sum_{m=1}^{M}q_{k'}b_{k'}c_{mk}^2\beta_{mk'}^2|\boldsymbol{\phi}_k^H\boldsymbol{\phi}_{k'}|^2 - \rho q_{k'}N\sum_{m=1}^{M}c_{mk}^2\beta_{mk'} \\
&= \rho q_{k'}N\sum_{m=1}^{M}\gamma_{mk}\beta_{mk'} - \rho q_{k'}N\sum_{m=1}^{M}c_{mk}^2\beta_{mk'} - \tau\rho_{\mathrm{p}}\rho N\sum_{m=1}^{M}q_{k'}b_{k'}c_{mk}^2\beta_{mk'}^2|\boldsymbol{\phi}_k^H\boldsymbol{\phi}_{k'}|^2. \qquad (49)
\end{aligned}
$$

REFERENCES

[1] J. Liu, M. Sheng, L. Liu, and J. Li, "Network densification in 5G: From the short-range communications perspective," *IEEE Commun. Mag.*, vol. 55, no. 12, pp. 96–102, Dec. 2017.

[2] E. Björnson, J. Hoydis, and L. Sanguinetti, "Massive MIMO networks: Spectral, energy, and hardware efficiency," *Found. Trends Signal Process.*, vol. 11, nos. 3–4, pp. 157–655, 2017.

[3] M. Rahmani, M. J. Dehghani, P. Xiao, M. Bashar, and M. Debbah, "Multi-agent reinforcement learning-based pilot assignment for cell-free massive MIMO systems," *IEEE Access*, vol. 10, pp. 120492–120502, 2022.

[4] H. Q. Ngo, A. Ashikhmin, H. Yang, E. G. Larsson, and T. L. Marzetta, "Cell-free massive MIMO versus small cells," *IEEE Trans. Wireless Commun.*, vol. 16, no. 3, pp. 1834–1850, Mar. 2017.

[5] A. M. Saray and A. Ebrahimi, "MAX-MIN power control of cell free massive MIMO system employing deep learning," in *Proc. 4th West Asian Symp. Opt. Millim.-Wave Wireless Commun. (WASOWC)*, 2022, pp. 1–4.

[6] Q. Wu and R. Zhang, "Towards smart and reconfigurable environment: Intelligent reflecting surface aided wireless network," *IEEE Commun. Mag.*, vol. 58, no. 1, pp. 106–112, Jan. 2020.

[7] X. Guo, Y. Chen, and Y. Wang, "Compressed channel estimation for near-field XL-MIMO using triple parametric decomposition," *IEEE Trans. Veh. Technol.*, vol. 72, no. 11, pp. 15040–15045, Nov. 2023.

[8] G. Torcolacci, N. Decarli, and D. Dardari, "Holographic MIMO communications exploiting the orbital angular momentum," *IEEE Open J. Commun. Soc.*, vol. 4, pp. 1452–1469, 2023.

[9] Y. Chen, Y. Wang, Z. Wang, and Z. Han, "Angular-distance based channel estimation for holographic MIMO," *IEEE J. Sel. Areas Commun.*, vol. 42, no. 6, pp. 1684–1702, Jun. 2024.

[10] M. Sarker and A. O. Fapojuwo, "Granting massive access by adaptive pilot assignment scheme for scalable cell-free massive MIMO systems," in *Proc. IEEE 93rd Veh. Technol. Conf.*, 2021, pp. 1–5.

[11] A. Ghazanfari, H. V. Cheng, E. Björnson, and E. G. Larsson, "Enhanced fairness and scalability of power control schemes in multi-cell massive MIMO," *IEEE Trans. Commun.*, vol. 68, no. 5, pp. 2878–2890, May 2020.

[12] T. Van Chien, E. Björnson, and E. G. Larsson, "Joint power allocation and user association optimization for massive MIMO systems," *IEEE Trans. Wireless Commun.*, vol. 15, no. 9, pp. 6384–6399, Sep. 2016.

[13] H. Yang and T. L. Marzetta, "Massive MIMO with max-min power control in line-of-sight propagation environment," *IEEE Trans. Commun.*, vol. 65, no. 11, pp. 4685–4693, Nov. 2017.

[14] S. Boyd and L. Vandenberghe, *Convex Optimization*. Cambridge, U.K.: Cambridge Univ. Press, 2004.

[15] M. Bashar, K. Cumanan, A. G. Burr, M. Debbah, and H. Q. Ngo, "On the uplink max–min SINR of cell-free massive MIMO systems," *IEEE Trans. Wireless Commun.*, vol. 18, no. 4, pp. 2021–2036, Apr. 2019.

[16] G. Liu, H. Deng, X. Qian, W. Zhang, and H. Dong, "Joint pilot and data power control for cell-free massive MIMO IoT systems," *IEEE Sensors J.*, vol. 22, no. 24, pp. 24647–24657, Dec. 2022.

[17] M. Zaher, O. T. Demir, E. Björnson, and M. Petrova, "Learning-based downlink power allocation in cell-free massive MIMO systems," *IEEE Trans. Wireless Commun.*, vol. 22, no. 1, pp. 174–188, Jan. 2023.

[18] C. F. Mendoza, S. Schwarz, and M. Rupp, "User-centric clustering in cell-free MIMO networks using deep reinforcement learning," in *Proc. IEEE Int. Conf. Commun. (ICC)*, 2023, pp. 1036–1041.

[19] G. Chen, S. He, Z. An, Y. Huang, and L. Yang, "A deep learning method: QoS-aware joint AP clustering and beamforming design for cell-free networks," *IEEE Trans. Commun.*, vol. 71, no. 12, pp. 7023–7038, Dec. 2023.

[20] Y. Al-Eryani, M. Akrout, and E. Hossain, "Multiple access in cell-free networks: Outage performance, dynamic clustering, and deep reinforcement learning-based design," *IEEE J. Sel. Areas Commun.*, vol. 39, no. 4, pp. 1028–1042, Apr. 2021.

[21] F. Fredj, Y. Al-Eryani, S. Maghsudi, M. Akrout, and E. Hossain, "Distributed beamforming techniques for cell-free wireless networks using deep reinforcement learning," *IEEE Trans. Cogn. Commun. Netw.*, vol. 8, no. 2, pp. 1186–1201, Jun. 2022.

[22] C. D'Andrea, A. Zappone, S. Buzzi, and M. Debbah, "Uplink power control in cell-free massive MIMO via deep learning," in *Proc. IEEE 8th Int. Workshop Comput. Adv. Multi-Sens. Adapt. Process. (CAMSAP)*, 2019, pp. 554–558.

[23] N. Rajapaksha, K. B. S. Manosha, N. Rajatheva, and M. Latva-Aho, "Deep learning-based power control for cell-free massive MIMO networks," in *Proc. IEEE Int. Conf. Commun. (ICC)*, 2021, pp. 1–7.
[24] N. Rajapaksha, K. B. S. Manosha, N. Rajatheva, and M. Latva-aho, "Unsupervised learning-based joint power control and fronthaul capacity allocation in cell-free massive MIMO with hardware impairments," *IEEE Wireless Commun. Lett.*, vol. 12, no. 7, pp. 1159–1163, Jul. 2023.
[25] Y. Zhang, J. Zhang, Y. Jin, S. Buzzi, and B. Ai, "Deep learning-based power control for uplink cell-free massive MIMO systems," in *Proc. IEEE Glob. Commun. Conf. (GLOBECOM)*, 2021, pp. 1–6.
[26] R. Nikbakht, A. Jonsson, and A. Lozano, "Unsupervised-learning power control for cell-free wireless systems," in *Proc. IEEE 30th Annu. Int. Sym. Pers., Indoor Mobile Radio Commun. (PIMRC)*, 2019, pp. 1–5.
[27] H. Ahmadi, A. Farhang, N. Marchetti, and A. MacKenzie, "A game theoretic approach for pilot contamination avoidance in massive MIMO," *IEEE Wireless Commun. Lett.*, vol. 5, no. 1, pp. 12–15, Feb. 2016.
[28] S. Mohebi, A. Zanella, and M. Zorzi, "Repulsive clustering based pilot assignment for cell-free massive MIMO systems," in *Proc. 30th Eur. Signal Process. Conf. (EUSIPCO)*, 2022, pp. 717–721.
[29] R. Chen, H. Wang, and R. Song, "Pilot assignment based on graph coloring with sum-rate Maximization in cell-free massive MIMO," in *Proc. 7th Int. Conf. Comput. Commun. (ICCC)*, 2021, pp. 1890–1894.
[30] J. Li, Z. Wu, P. Zhu, D. Wang, and X. You, "Scalable pilot assignment scheme for cell-free large-scale distributed MIMO with massive access," *IEEE Access*, vol. 9, pp. 122107–122112, 2021.
[31] T. C. Mai, H. Q. Ngo, and L.-N. Tran, "Design of pilots and power control in the cell-free massive MIMO uplink," in *Proc. 54th Asilomar Conf. Signals, Syst., Comput.*, 2020, pp. 831–835.
[32] L. Diao, J. Li, P. Zhu, D. Wang, and X. You, "Adaptive federated learning-based joint pilot design and active user detection in scalable cell-free massive MIMO systems," in *Proc. 4th Inf. Commun. Tech. Conf. (ICTC)*, 2023, pp. 232–236.
[33] *Study on Channel Model for Frequencies from 0.5 to 100 GHz, Version 17*, 3GPP Standard TS 38.901, Mar. 2022.
[34] M. U. Khan, E. Testi, M. Chiani, and E. Paolini, "Optimizing power control and pilot allocation in cell-free massive MIMO via deep learning," in *Proc. IEEE Int. Sym. Pers., Indoor Mobile Radio Commun.*, submitted for publication.
[35] I. Goodfellow, Y. Bengio, and A. Courville, *Deep Learning*. Cambridge, MA, USA: MIT Press, 2016. [Online]. Available: http://www.deeplearningbook.org.
[36] K. He, X. Zhang, S. Ren, and J. Sun, "Delving deep into rectifiers: Surpassing human-level performance on ImageNet classification," in *Proc. IEEE Int. Conf. Comput. Vis. (ICCV)*, 2015, pp. 1026–1034.
[37] D. P. Kingma and J. Ba, "Adam: A method for stochastic optimization," in *Proc. 3rd Int. Conf. Learn. Represent. (ICLR)*, 2015, pp. 1–15.
[38] O. T. Demir, E. Björnson, and L. Sanguinetti, "Foundations of user-centric cell-free massive MIMO," *Found. Trends Signal Process.*, vol. 14, nos. 3–4, pp. 162–472, 2021.
[39] X. Wu, *Performance Evaluation, Prediction and Visualization of Parallel Systems*, vol. 4. Boston, MA, USA: Kluwer Acad. Publ., 1999.

MUHAMMAD USMAN KHAN (Member, IEEE) received the B.S. degree in electrical engineering degree (cum laude) from the National University of Computer and Emerging Sciences, Lahore, Pakistan, in 2016, and the Master of Science degree (with Distinction) in advanced electronic systems engineering from the University of Kent, Canterbury, U.K., in 2018. He is currently pursuing the Ph.D. degree in electronics, telecommunications, and information technologies with the University of Bologna, Cesena, Italy. He worked as a Full-Time Faculty Member with the School of Computing, National University of Computer and Emerging Sciences. His research interest includes active users detection and channel estimation in a massive Internet of Things scenario using deep learning.

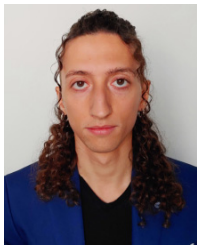

ENRICO TESTI (Member, IEEE) received the M.S. degree (magna cum laude) in electronics and telecommunications engineering for energy and the Ph.D. degree in electronics, telecommunications, and information technologies engineering from the University of Bologna, Italy, in 2018 and 2022, respectively, where he is currently a Junior Assistant Professor with the Department of Electrical, Electronic, and Information Engineering "Guglielmo Marconi." He is also Secretary/Treasurer of the IEEE ITSoc Italy Section Chapter. He has been affiliated with the National Laboratory of Wireless Communications, Italian National Inter-University Consortium for Telecommunications since 2020. His research interests include artificial intelligence techniques for next-generation wireless networks, massive MIMO, and satellite IoT.

MARCO CHIANI (Fellow, IEEE) received the Dr. Ing. degree (summa cum laude) in electronic engineering and the Ph.D. degree in electronic and computer engineering from the University of Bologna, Italy, in 1989 and 1993, respectively. He is a Full Professor of Telecommunications with the University of Bologna. Since 2003, he has been a Frequent Visitor with the Massachusetts Institute of Technology, Cambridge, where he currently holds a Research Affiliate appointment. His research interests are in the areas of information theory, wireless systems, statistical signal processing, and quantum information. He received the 2011 IEEE Communications Society Leonard G. Abraham Prize in the Field of Communications Systems, the 2012 IEEE Communications Society Fred W. Ellersick Prize, and the 2012 IEEE Communications Society Stephen O. Rice Prize in the Field of Communications Theory. He served as Elected Chair of the Radio Communications Committee of the IEEE Communication Society from 2002 to 2004 and as an Editor of Wireless Communication for the IEEE TRANSACTIONS ON COMMUNICATIONS from 2000 to 2007.

ENRICO PAOLINI (Senior Member, IEEE) received the Dr.Ing. degree (summa cum laude) in telecommunications engineering and the Ph.D. degree in electrical engineering from the University of Bologna, Italy, in 2003 and 2007, respectively.

While working toward the Ph.D. degree, he was a Visiting Research Scholar with the Department of Electrical Engineering, University of Hawai'i at Manoa, Honolulu, HI, USA. He was a Visiting Scientist with the Institute of Communications and Navigation, German Aerospace Center in 2012 and 2014, under DLR-DAAD fellowships. He is currently an Associate Professor with the Department of Electrical, Electronic, and Information Engineering, University of Bologna. His research interests include digital communication systems, error correcting codes, massive multiple access protocols, and detection and tracking in radar systems. He served as the Co-Chair for the ICC 2014, ICC 2015, and ICC 2016 Workshop on Massive Uncoordinated Access Protocols (MASSAP), the VTC 2019-Fall Workshop on Small Data Networks, the 2018 IEEE European School of Information Theory, and the 2020 IEEE Information Theory Workshop. He served as the TPC Co-Chair for the IEEE GLOBECOM 2022–Communication Theory Symposium and the IEEE GLOBECOM 2019–Communication Theory Symposium. He is the Chair of the ITSoc Italy Section Chapter and the Secretary of the IEEE ComSoc Radio Communications Committee. He was an Editor of IEEE COMMUNICATIONS LETTERS from 2012 to 2015 and the IEEE TRANSACTIONS ON COMMUNICATIONS (in coding and information theory) from 2015 to 2020.

Open Access funding provided by 'Alma Mater Studiorum - Università di Bologna' within the CRUI CARE Agreement